Chemical Physics Letters 637 (2015) 13–17

Contents lists available at ScienceDirect

Chemical Physics Letters

journal homepage: www.elsevier.com/locate/cplett

Entrance dynamics of CH_4 molecules through a methane–water interface

Ezequiel L. Murina [a], Claudio Pastorino [b], Roberto Fernández-Prini [a,c,*]

[a] Gerencia de Química, CAC-CNEA, Buenos Aires, Argentina
[b] Departamento de Física de la Materia Condensada, CAC-CNEA/CONICET, Buenos Aires, Argentina
[c] INQUIMAE, FCEN, UBA/CONICET, Buenos Aires, Argentina

ARTICLE INFO

Article history:
Received 5 June 2015
In final form 25 July 2015
Available online 31 July 2015

ABSTRACT

We studied the entrance mechanism of methane molecules into bulk water by Molecular Dynamics simulation over a broad time window. We corroborated that the presence of absorbed methane, under the studied thermodynamic state (298 K and roughly 10 MPa), does not influence the molecular configuration of water interface. Some representative interfacial trajectories were analyzed in detail and we propose an entrance mechanism in which interfacial water is not actively involved in the dissolution process. Finally, we described the Helmholtz Free Energy profile through the interface and obtained the dissolution free energy of methane in water.

1. Introduction

The interest in having a clear understanding of the interactions and configuration of the interfaces between water and a hydrophobic object is still a matter of intense research. The role played by the geometric features of the hydrophobic object is of significant importance. For instance, FDP [1] have clearly shown that for linear alkanes the effect of solvent on their configurations is almost nil, at least up to twenty carbons. Graziano supported this view [2], using a scaled particle theory for spherocylinders. He showed that linear alkanes dissolved in water remain essentially in a configuration akin to a necklace of CH_2 groups which extends up to fifty carbons. On the other hand, Chandler and co-workers have studied the subject in a very important series of papers, showing that this is not the case for hydrophobic surfaces or for three dimensional hydrophobic solutes in contact with water [3–5]. Hence, there is a notable difference in bulky configuration for dissolved hydrophobic objects of different dimensionality.

In order to inquire into the dynamics of penetration of hydrophobic solutes to become dissolved in water, it seems important to be able to describe the trajectory of the solutes as they enter the bulk water phase, and we chose therefore the simplest alkane CH_4. Ghoufi and co-workers have recently shown that methane molecules adsorb on the water–methane interface [6] and proposed a simple schematic model for the penetration of methane molecules dissolving in water. Their dissolution scheme is close to that proposed by Knox and Phillips [7], which corresponds to a quasi-chemical step-wise reaction i.e. a more chemical model. Somasundaram et al. [8] studied two simple hydrophobic solutes and also CO_2 to understand the kinetics of gas uptake. They confirmed that there is a free energy minimum, indicative of a surface adsorption region for the hydrophobic solute. In addition, at least for N_2 and CO_2, a free energy barrier exists that hinders the adsorbed molecules from entering liquid water. We were interested in a description of the trajectories of CH_4 molecules that adsorb on the interface but do not enter bulk water predominantly and their comparison with the trajectories of the few that are finally dissolved in water. For this purpose, we used molecular dynamics simulations as described below.

2. Models and simulation technique

Our simulation system has two components: H_2O and CH_4. Water was simulated by means of the SPC/E [9] effective H_2O—H_2O intermolecular potential. We used for the intermolecular interactions between methane molecules the OPLS potential of Jorgensen [10]. This is a simple Lennard–Jones model of neutral spherical molecules with implicit hydrogens having a diameter $\sigma = 0.370$ nm and the depth of the potential well being $\varepsilon = 1.23\ \mathrm{kJ\,mol^{-1}}$. The cross-interaction parameters were calculated using the geometric mean for the energy and size parameters, which, in this case, yield values that are very close to those obtained with the

* Corresponding author at: Av. Gral. Paz 1499, Buenos Aires, Argentina.
E-mail address: rfernandezprini@cnea.gov.ar (R. Fernández-Prini).

http://dx.doi.org/10.1016/j.cplett.2015.07.045
0009-2614/

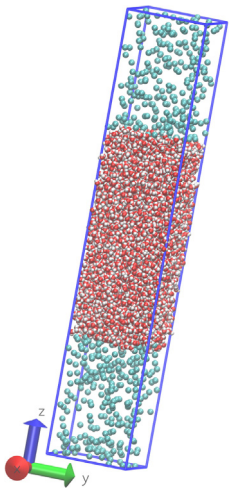

Figure 1. A configuration of the studied system as obtained from the simulations. In the center, the liquid phase of water molecules can be observed (red and light grey), between two volumes of methane molecules (blue white), which define two water–methane interfaces. Periodic boundary conditions were used in the three directions. (For interpretation of the references to color in this figure legend, the reader is referred to the web version of this Letter.)

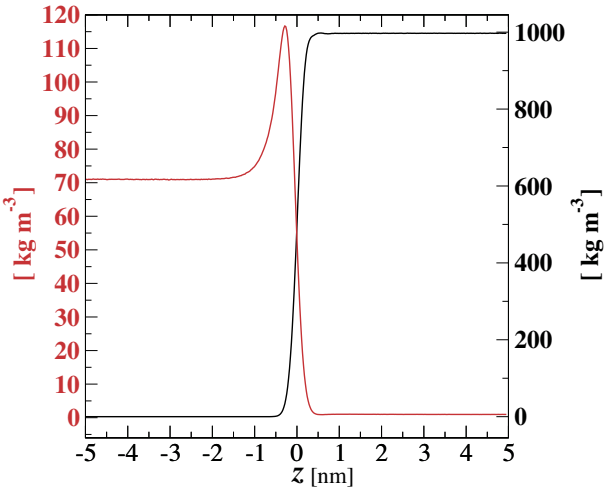

Figure 2. Density of methane (red line) and water (black line) along z axis perpendicular to the interface. At $z = 0$ is the Gibbs surface for water. (For interpretation of the references to color in this figure legend, the reader is referred to the web version of this Letter.)

Lorentz–Berthelot combination rule. The simulation box had a square base of 16 nm^2. In the middle of the box, we put a water slab of 12 nm height with 5367 H_2O molecules. Above and below this slab there were 5 nm compartments having 274 methanes each, as shown in Figure 1. In both phases the amount of the other component was very small and did not change, in essence, the main behavior of the dominant component.

The simulation box had periodic 3D boundary conditions, and the MD simulations were done with the Gromacs 4.6.5 molecular dynamics package [11]. The canonical ensemble (*NVT*) was used at a temperature of 298 K, fixed with the Nosé–Hoover thermostat [12]. We estimated the average partial pressure of methane to be around 10 MPa. To avoid slow diffusion of the water–methane interfaces, we fixed the center of mass of the water slab to the geometrical center of the simulation box. The electrostatic interactions among H_2O molecules were calculated applying the Particle Mesh Ewald method [13] with a mesh spaced 0.12 nm and a cutoff of 1.3 nm in real space. The equations of motion were integrated with the Leapfrog algorithm having a time step of 1 fs [14]. In order to fix the atomic bond distances of water we used the Settle algorithm [15]. We performed significantly long MD runs of 1000 ns for the complete system, and shorter simulations of 240 ns for pure water, storing the configurations every 1 ps. Typically we obtained 10^6 different configurations for the two-component system and 2.4×10^5 for pure water. These allowed us to obtain good average values for the physico-chemical quantities of interest.

Table 1 shows our simulation results for the properties of CH_4 dissolved in water, compared with those obtained by other authors by simulation and with experimental values, whenever available. We conclude that for equilibrium properties in bulk water, our simulation technique is quite satisfactory.

3. Interfacial properties of the studied system

The density profiles of each component along the z axis of the cell are plotted in Figure 2. Due to the long simulated time window, our result have very low statistical error.

A higher concentration of methane was observed at the interface. The degree of coverage of adsorbed methane is about 60% of the number of methanes, corresponding to a monolayer. These methane molecules are attractively adsorbed on the water–methane interface within a slab of *ca.* 1 nm wide. Beyond that distance, a repulsion of methanes from the interface sets up, generating a repulsive barrier for penetration of gas molecules into bulk water.

In agreement with Willard and Chandler [5], we have confirmed that the presence of the adsorbed hydrocarbon has no effect on the interfacial structure and configuration. This is shown in Figure 3, where the bidimensional pair correlation functions of O—O are plotted for two equivalent systems with and without methane. Equivalent systems are those with the same geometry and equal number of water molecules, simulated under identical thermodynamic conditions. The two-dimensional pair correlation functions were calculated for bins of 0.05 nm wide in z-direction, located progressivelly through the interfacial region and starting in the methane-rich zone of the two external compartments. In order to do that, we located the Gibbs dividing surface for the water given by the position where the average water density is half its bulk value. Three parallel planes were defined above and also below the Gibbs surface, spacing them by 0.05 nm. Inside the 6 slabs delimitated by two of these consecutive planes (including the Gibbs surface plane), the 2D pair correlation functions defined by

$$g_{2d}(r) = \sum_{i \neq j} \frac{\delta(r_{ij} - r)}{\rho} \tag{1}$$

Table 1
Physico-chemical properties of methane and water calculated to test the computational technique. We used the Test Particle Insertion Method [14] to measure the excess chemical potential of methane in water.

	Our simulations	Others simulations	Experimental values
Water bulk density (kg m^{-3})	994.8 ± 0.5	994 [16]	997 [17]
Excess chemical potential of methane in water (kJ mol^{-1})	24.6 ± 0.3	23.4 [18]	26.239 [19], 26.16 [20]
Solubility (10^{-5} mole fraction)	4.862 ± 0.001	7.869 [18]	2.5170 [19], 2.64 [20]
Radial distribution function O—O First Peak (nm)	0.276 ± 0.003	0.27 [21]	
Radial distribution function O—O Second Peak (nm)	0.449 ± 0.006	0.44 [21]	

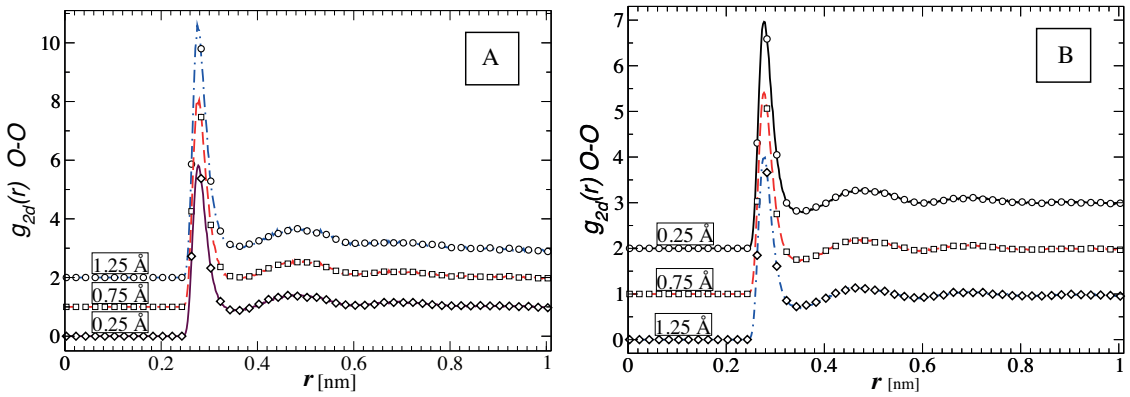

Figure 3. Bidimensional pair correlation functions of O—O for two equivalent systems, one with methane (curves) and the other without methane (symbols). Labels indicate the distance from the Gibbs water surface up to the center of each region, where $g_{2d}(r)$ was measured. Panel A corresponds to regions located above the Gibbs plane and panel B to regions located below that plane. For a better visualization, all functions were displaced on the ordinate axis and symbols were represented every 9 measured points.

were measured. Here ρ stands for the instantaneous local density of water in the zone of interest. From the agreement of $g_{2d}(r)$ in all the slabs of both equivalent systems in each region, we conclude that the presence of methane does not change the structure of the water interface.

In Figure 4, we present a detailed view of the functions $g_{2d}(r)$ in each studied slab. The displacement towards lower r values for the inner slabs strongly suggests that water in the external interfacial region is less structured than in the bulk liquid [22].

4. Dynamics of penetration

In the Supplementary Material we include two videos. The first one shows adsorbed methanes that try to enter into bulk water but are rejected by the water surface, and a single CH_4 molecule that does dissolve in bulk solution (representative of 31 penetration events observed in the simulations). For studying the entrance mechanism, we took 0.2 nm width water slabs with the z axis perpendicular to the interfaces (see Figure 1), one of them above the Gibbs surface and the others below it. Slabs are indicated in different colors and only O atoms of the water molecules are displayed. The second video shows each individual slab in a different panel and so we could observe the dynamics of methane and water molecules layer by layer (see Figure 5).

Visual inspection of the methane molecules in the different slabs, composed mainly by water molecules, evidence that methanes molecules place themselves in large quasi-cavities (empty spaces) formed by spontaneous water density fluctuations.

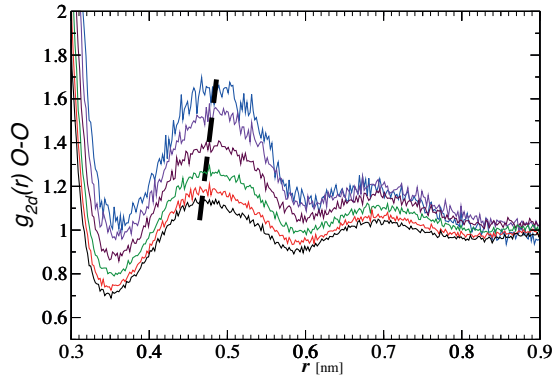

Figure 4. Detailed view of the overlapping curves corresponding to the system with methane (without displacing the ordinate axis) of Figure 3. Curves with the higher maxima correspond to the outer layers of interfacial water. The dashed line indicates a displacement of the functions towards lower r values.

As expected, the quasi-cavities decrease in size in the inner layers, as their densities are progressively closer to bulk water density. Figure 5 shows representative snapshots of these slabs. Up to the third layer, methanes located inside the quasi-cavities, at a distance from the first water neighbors of roughly one H_2O molecular diameter. Once methanes are able to proceed to the fourth slab, after a short time dangling close to it, they will finally penetrate into bulk water (see Video 1 in Supplementary Material).

5. Excess free energy

The symmetry of the simulated system allowed us to study the two interfaces at once for every MD simulation run (see Figure 1). Consequently, we had 2×10^6 different configurations for studying the methane/water interface. This implied that the statistics was increased sufficiently to measure a free energy profile through the interface without using methods of biased sampling, such as umbrella sampling [14]. We calculated the average probability density of methane localization $P(z)$ along the simulation box. As suggested by Somasundaran et al. [8,23], $P(z)$ is related to the Helmholtz Free Energy $A(z)$ by:

$$\frac{A(z)}{kT} = -\ln \rho(z) + \frac{A(z_0)}{kT} \tag{2}$$

where z is the position of methane with respect to an axis normal to interface, $A(z_0)$ is the Helmholtz Free Energy in the gaseous phase far from the interfacial region, T is the temperature and k is the Boltzmann constant.

Figure 6 shows the free energy profile along the interface. The uncertainty bars have a maximum value of 0.1 kJ mol^{-1} which is of the order of symbols' size. There is a minimum value of free energy in the region where methanes are adsorbed. The depth of this minimum is about -1.2 kJ mol^{-1}. The curve reaches a maximum value for a z value roughly corresponding to the position of the fourth water layer visualized in the videos of the Supplementary Material. There is an approximate 0.3 kJ mol^{-1} barrier for methanes that pass from the inner solution to the adsorbed phase. Somasundaram et al. saw a similar barrier in the case of C_2O molecules [8]. The solvation energy of methane in water is (10.6 ± 0.1) kJ mol^{-1}. When methane gas is considered at the standard pressure of 0.1 MPa, solvation energy becomes 22.02 kJ mol^{-1}. The inset plot shows a curve corresponding to the term $-\ln P^*(z) + \ln P^*(z_0)$, where $P^*(z)$ is the average localization probability density at the z position of those methanes that have been dissolved at least once during the MD simulation. In bulk regions, the curves are constant and roughly equal at both sides of the interface. This is an evidence that the

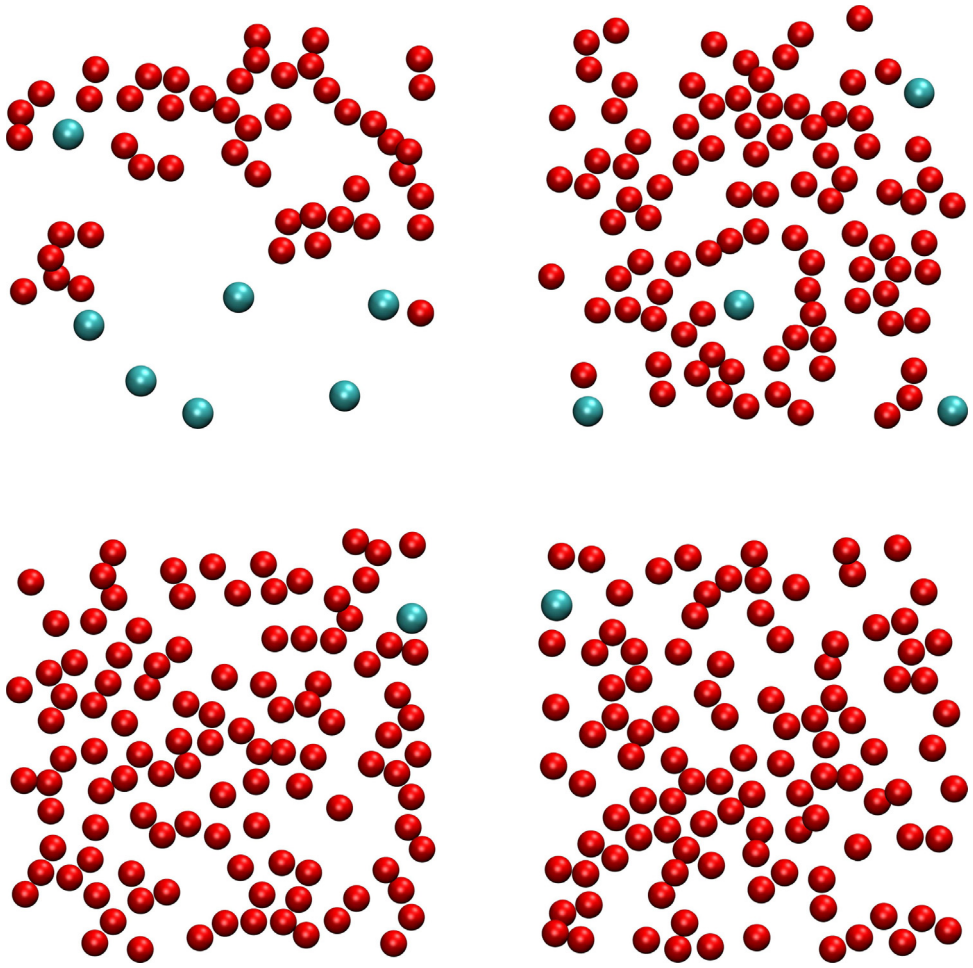

Figure 5. Representative snapshots of the methane/water interface in different consecutive slabs of 0.2 nm. Methanes are displayed in light blue and O atoms of water molecules in red. Top row: first slab, above the Gibbs dividing surface (left panel) and second slab, below it (right panel). Bottom row: third slab (left panel) and fourth slab where a methane that penetrates to the bulk water is showed (right panel). (For interpretation of the references to color in this figure legend, the reader is referred to the web version of this Letter.)

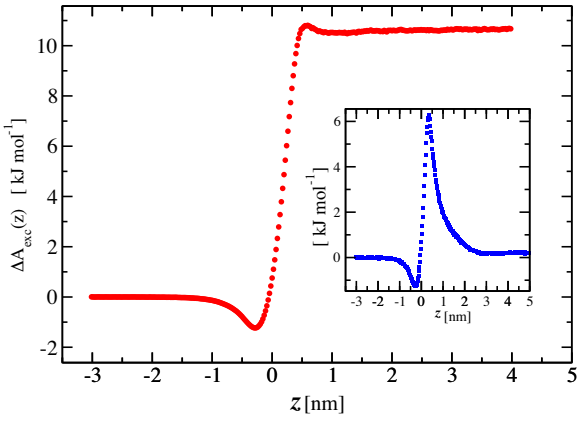

Figure 6. Excess Helmholtz Free Energy profile for methanes molecules along the simulation cell. Inset shows the term $-\ln P^*(z)+\ln P^*(z_o)$ for methanes that have been dissolved during the MD simulation. At $z=0$ is the Gibbs surface for water. The liquid phase is located at $z>0$.

simulated system has reached the equilibrium, within our simulation uncertainty which is very small.

6. Conclusions

Our MD simulation study confirms the observation of Willard and Chandler [5] that a hydrophobic object does not modify the water interface. This observation implies that the penetration of CH_4 into the bulk water is not due to adjustments of the aqueous interfacial layers around methane molecules. Consequently, previous models of the methane dissolution in bulk water which depict a gas molecule being increasingly surrounded by interfacial water, do not correctly represent the penetration phenomenon. Those models [6,7] are of a more chemical nature in the sense that the entrance of the hydrophobic solute involves a series of steps that consist of its progressive hydration by H_2O. According to our careful analysis of the trajectories of CH_4 molecules, we proposed the following entrance mechanism: CH_4 molecules that proceeding from the gas phase towards bulk solution, cross the interfacial region through quasi-cavities due to spontaneous water density fluctuations. The entrance of methane into bulk water appears to occur successfully when the CH_4 is able to penetrate a depth greater than 0.6 nm from the Gibbs plane. This depth corresponds to the z value at which the curve of free energy reaches a maximum value and also corresponds roughly to the localization of the fourth water layer showed in Figure 5.

Acknowledgements

The authors are grateful to Professor M. Laura Japas for useful discussions about the contents of this Letter. Financial support was obtained from the ANPCyT (Program PICT-2011-2378). E.L.M. received a fellowship from the same institution, CP. and

R.F-P. are members of the Carrera del Investigador (CONICET, Arg.).

Appendix A. Supplementary data

Supplementary data associated with this article can be found, in the online version, at http://dx.doi.org/10.1016/j.cplett.2015.07.045

References

[1] A.L. Ferguson, P.G. Debenedetti, A.Z. Panagiotopoulos, J. Phys. Chem. B 113 (2009) 6405.
[2] G. Graziano, Chem. Phys. Lett. 511 (2011) 262.
[3] K. Lum, D. Chandler, J.D. Weeks, J. Phys. Chem. B 103 (1999) 4570.
[4] D. Chandler, Nature 437 (2005) 640.
[5] A.P. Willard, D. Chandler, J. Chem. Phys. 141 (2014).
[6] A. Ghoufi, P. Malfreyt, Phys. Chem. Chem. Phys. 12 (2010) 5203.
[7] C.J.H. Knox, L.F. Phillips, J. Phys. Chem. B 102 (1998) 8469.
[8] T. Somasundaram, R.M. Lynden-Bell, C.H. Patterson, Phys. Chem. Chem. Phys. 1 (1999) 143.
[9] H.J.C. Berendsen, J.R. Grigera, T.P. Straatsma, J. Phys. Chem. 91 (1987) 6269.
[10] W.L. Jorgensen, J.D. Madura, C.J. Swenson, J. Am. Chem. Soc. 106 (1984) 6638.
[11] B. Hess, C. Kutzner, D. van der Spoel, E. Lindahl, J. Chem. Theory Comput. 4 (2008) 435.
[12] S. Nosé, J. Chem. Phys. 81 (1984) 511.
[13] U. Essmann, L. Perera, M.L. Berkowitz, T. Darden, H. Lee, L.G. Pedersen, J. Chem. Phys. 103 (1995) 8577.
[14] D. Frenkel, B. Smit, Understanding Molecular Simulation, Academic Press, Boston, 1996.
[15] S. Miyamoto, P.A. Kollman, J. Comput. Chem. 13 (1992) 952.
[16] C. Vega, E. de Miguel, J. Chem. Phys. (2007) 126.
[17] M.L.H.E.W. Lemmon, M. McLinden, NIST Standard Reference Database 23, version 8.0, Physical and Chemical Properties Division, NIST, Boulder, CO, 2007.
[18] D. Paschek, J. Chem. Phys. 120 (2004).
[19] T.R. Rettich, Y.P. Handa, R. Battino, E. Wilhelm, J. Phys. Chem. 85 (1981) 3230.
[20] J.L. Alvarez, R. Fernández Prini, J. Solut. Chem. 37 (2008) 1379.
[21] A.K. Soper, F. Bruni, M.A. Ricci, J. Chem. Phys. 106 (1997) 247.
[22] I.-F.W. Kuo, C.J. Mundy, Science 303 (2004) 658.
[23] C. Chipot, M.A. Wilson, A. Pohorille, J. Phys. Chem. B 101 (1997) 782.